Meteorologische Zeitschrift, Vol. **14**, No. 6, 755-762 (December 2005)

Article

EMAD: an empirical model of air-sea fluxes

JIN-SONG VON STORCH[1], JUAN PEDRO MONTAVEZ[2] and BALAN SAROJINI BEENA[1]

[1]Institute of Meteorology, University of Hamburg, Hamburg, Germany
[2]Universidad de Murcia, Departamento de Fisica, Universidad de Murcia, Murcia, Spain

(Manuscript received March 8, 2005; in revised form September 6, 2005; accepted October 10, 2005)

Abstract

An empirical model of daily fluxes at the sea surface is proposed. The model, referred to as EMAD (Empirical Model of Atmospheric Dynamics), concentrates on the linear dynamics of the time-varying part of the air-sea fluxes. It is based on a general formulation that allows different types of air-sea interactions depending on the relative dominance of the model parameters. The parameters are obtained by fitting the model to a long integration with a coupled atmosphere ocean general circulation model. EMAD is able to reproduce air-sea interactions found in a coupled general circulation model. In particular, EMAD reveals realistic stationary responses to different sea surface conditions. The variance distributions produced by EMAD are comparable to those obtained from an integration with a coupled general circulation model. Finally, the characteristic air-sea interactions as described by the cross-correlation functions and found in an integration with a coupled general circulation model are captured by EMAD. Given these properties of EMAD, the ocean circulation and its variability can be studied using an ocean general circulation model driven by EMAD.

Zusammenfassung

Ein empirisches Modell der Flüsse an der Grenzfläche zwischen Atmosphäre und Ozean wird vorgestellt. Das als EMAD (Empirical Model of Atmospheric Dynamics) bezeichnete Modell beschreibt die lineare Dynamik des zeitlich variierenden Teils der Flüsse. Es basiert auf einer allgemeinen Formulierung, die je nach den Parameterwerten verschiedene Typen der Atmophäre-Ozean-Wechselwirkungen beschreiben kann. Die Parameter sind an eine Langzeitintegration mit einem gekoppelten Atmosphäre-Ozean-Zirkulationsmodell angepasst. Es wird gezeigt, dass das EMAD-Modell in der Lage ist, die im gekoppelten Zirkulationsmodell identifizierten Wechselwirkungen zu reproduzieren. Insbesondere reagiert das EMAD realistisch auf unterschiedliche Bedingungen an der Meeresoberfläche. Die Varianzen der EMAD-Flüsse sind mit den der durch das gekoppelte Zirkulationsmodell erzeugten Flüsse vergleichbar. Ferner sind die Charakteristiken der Wechselwirkungen, die sich durch Kreuzkorrelationsfunktionen beschreiben lassen, von EMAD reproduziert. In Anbetracht dieser Eigenschaften des Modells können die Ozeanzirkulation and deren Variabilität mit Hilfe eines durch das EMAD-Modell angetriebenen Ozean-Zirkulationsmodells untersucht werden.

1 Introduction

When studying the ocean using an ocean general circulation model (O-GCM), one has to specify first the fluxes of heat, fresh water and momentum at the sea surface, that drive the ocean model. Hereafter, these fluxes are denoted by **H**, **F** and **M** respectively (bold letters indicate vectors). They can be decomposed into climatological mean annual cycles, $\mathbf{H}_c$, $\mathbf{F}_c$ and $\mathbf{M}_c$, and deviations from the climatological annual cycles, $\mathbf{H}^{'}$, $\mathbf{F}^{'}$ and $\mathbf{M}^{'}$.

The fluxes can be modeled either with the aid of parameterizations implemented in an A-GCM, or using ad hoc assumptions in form of strongly simplified atmospheric models. A widely used simple formulation is

$$\mathbf{H}_t = \alpha(\mathbf{T}^* - \mathbf{T}_t) = \mathbf{H}_c - \alpha\mathbf{T}_t^{'}, \quad \mathbf{F}_t = \mathbf{F}_c, \quad \mathbf{M}_t = \mathbf{M}_c. \quad (1.1)$$

$\mathbf{H}_t$ is obtained by restoring SST, $\mathbf{T}_t$, to a prescribed temperature (apparent atmospheric equilibrium temperature or simply the observed SST), $\mathbf{T}^*$, with a restoring coefficient α. $\mathbf{H}_c$ equals $\alpha(\mathbf{T}^* - \mathbf{T}_c)$ and is obtained by decomposing **T** into its climatological mean annual cycle, $\mathbf{T}_c$, and the deviation from $\mathbf{T}_c$, $\mathbf{T}^{'}$. The first two expressions in Eq.(1.1) represent the so-called mixed boundary condition. Another example along this line is the formulation used by LATIF and VILLWOCK (1990)

$$\mathbf{H}_t = \mathbf{H}_c, \quad \mathbf{F}_t = \mathbf{F}_c, \quad \mathbf{M}_t = \mathbf{M}_c + \mathscr{L}\,\mathbf{T}_t', \quad (1.2)$$

where $\mathscr{L}$ is a matrix estimated from data. Both $\mathbf{H}_t = \mathbf{H}_c - \alpha\mathbf{T}^{'}$ in Eq.(1.1) and $\mathbf{M}_t = \mathscr{L}\,\mathbf{T}_t'$ in Eq.(1.2) rely on the assumption that the atmosphere, after being perturbed by an SST anomaly, can quickly reach a quasi-stationary state so that the fluxes can be considered as direct responses to the SST anomaly.

While a coupled AO-GCM produces both the climatological and the time-varying components of the fluxes at costs of heavy computations, simple models such as Eq.(1.1) or Eq.(1.2) prescribe the climatological components (denoted by $\mathbf{H}_c$, $\mathbf{F}_c$ and $\mathbf{M}_c$ in Eq.(1.1) and Eq.(1.2)) at almost no additional computational costs.

*Corresponding author: Jin-Song von Storch, Institut für Meteorologie, Universität Hamburg, Bundesstraße 55, 20146 Hamburg, Germany, e-mail: jin-song.storch@dkrz.de

0941-2948/2005/0080 $ 3.60

DOI: 10.1127/0941-2948/2005/0080

This makes the simple models attractive, provided that they are able to produce time-varying components of the fluxes realistically. Unfortunately, many simple models, including Eq.(1.1) and Eq.(1.2), cannot represent the time-varying components of the fluxes satisfactorily. In particular, they do not describe variations originating from the atmospheric motions.

To demonstrate this, consider the cross-covariance function between a flux at a grid point, x, and an oceanic variable (e.g. SST) at the same grid point, y,

$$R_{xy}(\tau) = \overline{x'_t y'_{t+\tau}}, \tag{1.3}$$

where $\bar{}$ indicates the time average. τ indicates the time lag and x' and y' denote deviations from the corresponding climatological mean annual cycles. R_{xy} is not always symmetric about $\tau = 0$ and can be used to distinguish the situation when x leads (i.e. $\tau > 0$), from the situation when y leads (i.e. $\tau < 0$). Different air-sea interactions are characterized by different shapes of covariance functions. Fig. 1 shows covariance functions related to three types of air-sea interactions. The cross-covariance function indicated by the thin solid line in Fig. 1 is obtained when x' responds to y' occurring at an early time $t - \Delta$ such that $x'_t = const \times y'_{t-\Delta}$. Multiplying $x'_t = const \times y'_{t-\Delta}$ by $y'_{t+\tau}$ and applying the average operator $\bar{}$ on the result, one finds $R_{x,y} = const\, R_{yy}(\tau + \Delta)$ which peaks at time lag $-\Delta$ when y leads and is symmetric about $-\Delta$. When $\Delta = 0$ is assumed, as for **H** in Eq.(1.1) and for **M** in Eq.(1.2), $R_{xy}(\tau)$ would be symmetric about $\tau = 0$. The thick gray line in Fig. 1, on the other hand, describes the situation when y' is generated by x', and after being generated, y' does not feedback to x'. In this case, $R_{x,y}$ peaks when x' leads and is zero when y' leads. The detailed shape of $R_{x,y}$ depends on the memory of x' and y'. Finally the dashed line in Fig. 1 describes the situation when y' is first generated and then damped by x', which leads to an anti-symmetric $R_{x,y}$ (FRANKIGNOUL, 1985). A more general discussion on various types of interactions is given by VON STORCH (2000).

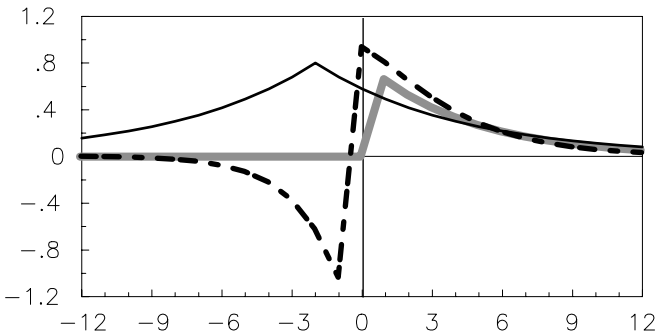

Figure 1: Covariance functions characterize three idealized types of air-sea interactions. Positive (negative) time lags in months correspond to the situation when atmosphere leads (ocean leads).

In reality, the relation between momentum flux and SST and between heat flux and SST are seldom described by a symmetric covariance function as suggested by Eq.(1.1) and Eq.(1.2). FRANKIGNOUL et al. (1998) showed that R_{HT} in extratropics is antisymmetric and resembles the dashed line in Fig. 1. VON STORCH (2000) showed that this type of covariance functions also prevails in most of the extratropical regions in an integration with the coupled ECHAM3/LSG AO-GCM. Furthermore, it was found that covariance functions between wind stress and SST in the mid- and high-latitude regions in the coupled GCM resemble the gray line in Fig. 1. Even in the tropical Pacific, R_{MT} is not strictly symmetric, indicating more complicated feedbacks between SST and wind stress than a pure stationary response of wind stress to SST. One has to conclude that the complex nature of air-sea interactions can so far only be captured by an A-GCM, but not by the simple models mentioned above.

This paper aims to develop a simple model that captures the complex nature of air-sea interactions. The main difference between the present approach and the simple models (1.1) and (1.2) is that the model is not built on one particular assumption, but is described by a general form which allows different types of interactions, depending on model parameters. The model is empirical, since the model parameters are obtained by fitting the model into an integration with a coupled AO-GCM. It consists of a deterministic part and a noise part. The former describes the linear dynamics of the fluxes and the linear responses of fluxes to sea surface conditions. The model aims to reproduce the variances found in an A-GCM and furthermore, when coupled to an O-GCM, to reproduce the same types of covariance functions, as found in the coupled AO-GCM. It can be considered as statistically equivalent to an A-GCM with respect to second moments of the time-varying surface fluxes. As the model is empirical and captures the linear dynamics of air-sea interaction, it will be referred to as EMAD (Empirical Model of Atmospheric Dynamics).

A description of EMAD is given in Section 2. To analyze the performance of EMAD, the response of EMAD to different anomalous sea surface conditions is studied in Section 3. Since EMAD with a noise term is not optimal in predicting individual fluxes for a given sea surface condition, Section 4 concentrates on the ability of EMAD in producing the realistic flux statistics, i.e. the total variances and the cross-correlation functions between fluxes and the SST which represent different types of air-sea interactions. For this purpose, uncoupled EMAD integrations and an integration of EMAD coupled to HOPE-G O-GCM are considered. It will be shown that the important types of air-sea interactions identified in the coupled AO-GCM are captured by the EMAD model. A summary is given in the final Section.

2 Model description

The model parameters are derived from a control integration with the ECHO-G AO-GCM (LEGUTKE and VOSS, 1999). The resolution for the atmosphere is T30. For the ocean, T42 resolution with equatorial refinement is used. An integration with essentially the same coupled model is discussed by RAIBLE et al. (2001).

EMAD is an anomaly model. All variables considered represent deviations from the climatological mean annual cycle. For the sake of shortness, $'$ is dropped hereafter. Based on the assumption that the time-varying fluxes represent small deviations from their climatological annual cycle, EMAD is proposed to have the following linear form

$$\mathbf{x}_{t+1} = \mathscr{A}\mathbf{x}_t + \mathscr{B}\mathbf{y}_t + \mathscr{C}\mathbf{n}_{t+1}. \qquad (2.1)$$

x consists of all fluxes required to drive an OGCM. It includes in addition to the net fluxes of heat, fresh water and momentum also specific fluxes, such as the short wave radiation used to describe the penetration of solar radiation into the ocean, the conductive and the residual heat flux used to describe the sea ice. **y** represents the oceanic variables at the sea surface, such as the SST and the sea ice cover, that can affect **x**. The matrix $\mathscr{A}$ depicts the linear behavior of the fluxes, $\mathscr{B}$ the linear responses of the fluxes to oceanic anomalies at the sea surface, and $\mathscr{C}$ the covariance structure of the part of **x** that is not captured by $\mathscr{A}$ and $\mathscr{B}$. **n** is a white noise. The stochastic forcing $\mathscr{C}\mathbf{n}$ is white in time, but not in space.

Equation (2.1) suggests that EMAD is able to describe different types of air-sea interactions. If the second term on the right hand side of Eq.(2.1) dominates, EMAD would only produce linear responses of **x** to **y**, just as Eq.(1.1) and Eq.(1.2). On the other hand, if the second term is negligible, the fluxes would generate variations in **y**. However, once being generated, **y** would not feedback to **x**. Covariance functions resembling the gray line in Fig. 1 would be observed. Finally, if the three terms on the right hand side of Eq.(2.1) are of comparable strength, **y** would be generated by the fluxes. Once being generated, **y** would feedback to the fluxes. The cross-correlation function related to this type of air-sea interactions is described by the dashed line in Fig. 1. Generally, the relative importance of the three terms varies geographically and depends on which flux is considered.

Eq.(2.1) represents only the general form of EMAD. In practice, the model has a much more complicated structure. It operates in two spaces and has two modules.

2.1 a) Two spaces of EMAD

The number of ocean grid points in the ECHAM4 T30 model is 3056. Thus, the dimensions of **x** and **y** are easily of the order of 10^4. In order to avoid overfitting and furthermore to simplify the estimation procedure, the data are first compressed. This leads to the usage of a reduced EOF-space and the full grid-point space. $\mathscr{A}$ and $\mathscr{B}$ are estimated in the reduced space spanned by the leading EOFs. The fluxes produced by the deterministic part of EMAD, $\mathscr{A}\mathbf{x}_t + \mathscr{B}\mathbf{y}_t$, are then transformed back to the grid-point space, where the stochastic forcing $\mathscr{C}\mathbf{n}$ is added. $\mathscr{C}$ represents the covariance structure of the errors which are not described by $\mathscr{A}$ and $\mathscr{B}$ and have much smaller spatial scales than fluxes produced by the deterministic part of EMAD. This matrix is obtained in the grid-point space and for each flux separately. The final output of EMAD are fluxes at all grid points.

Note that the general EMAD ansatz (2.1) allows for both non-local and local relationships. The relationship at a grid point is more non-local, if the contribution from $\mathscr{A}$ and $\mathscr{B}$ terms dominate that from $\mathscr{C}$ term, and vice versa, if the contribution of $\mathscr{C}$ term dominates.

The EOFs are calculated for the daily time series for each fluxes in **x** and for each variables in **y**. With increasing number of EOFs, the ability of EMAD in predicting ECHO-G-fluxes increases, as suggested by the correlation skill (not shown). This is particularly true when the numbers of EOFs used are small. For the EMAD presented below, the number of EOFs chosen is 100 for each flux in **x** and for each oceanic variable in **y** in water module and 50 in ice module. The modules are defined below. Each EOF included explains at least 0.25% of the total variance of the respective variable. The cumulative variances explained by these EOFs range from 50 to 80% for different fluxes. Note that since daily data are used, the leading EOFs for fluxes represent synoptic-scale variations and explain only a few percentages of the respective total variances.

b) Two modules of EMAD

The air-sea coupling in ice-free regions differs from that in regions where sea ice can be formed. As a consequence, the surface fluxes as well as the oceanic conditions that affect the fluxes are different in the two regions. To describe these different coupling processes, two modules are used. The water-module is defined in regions where sea ice cannot be found all year round and the ice-module is defined in regions where the formation of sea ice is permitted. The boundary is derived from the ECHO-G-integration and fixed afterwards. For each of the two modules, a set of matrices $\mathscr{A}$, $\mathscr{B}$ and $\mathscr{C}$ is derived.

The main difference between the two modules is that the ice-module contains much more fluxes than the water module. First of all, one has to consider the residual and conductive heat flux required to describe the formation or melting of the ice. In addition to that, since a grid cell in the domain of the ice-module contains an ice-covered and ice-free part where different dynamics take

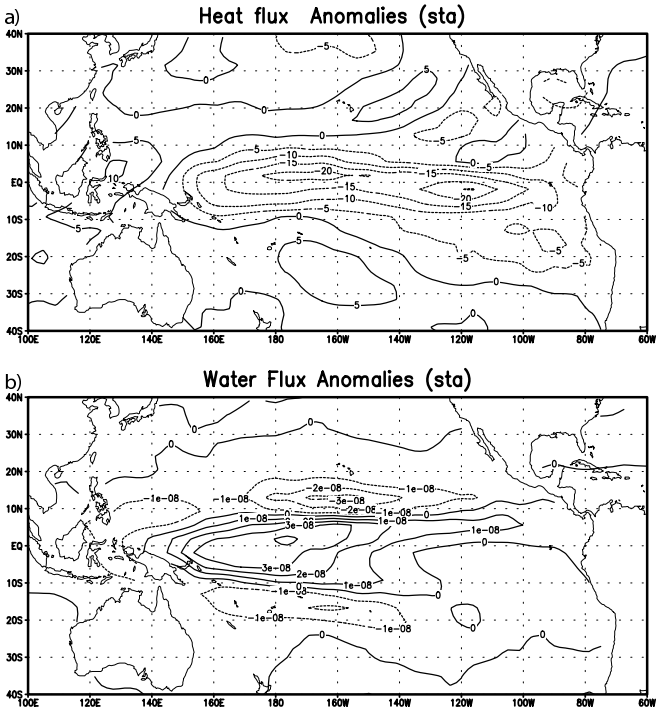

Figure 2: Stationary responses of EMAD to El Nino SST anomalies in terms of the net heat flux (W/m^2) in a) and the net fresh water flux (m/s) in b).

place, fluxes over ice-covered and ice-free part of a grid cell have to be treated separately. In general, $\mathbf{x}$ in a cell in the domain of the ice module consists of $\mathbf{x}^{free}$ and $\mathbf{x}^{ice}$. The former enters the ocean beneath the ice-free part of the cell, whereas the latter interacts with the sea ice. The net flux in a grid cell is

$$\mathbf{x}_t = \mathrm{A}_t \mathbf{x}_t^{ice} + (1 - \mathrm{A}_t)\mathbf{x}_t^{free}, \qquad (2.2)$$

A_t is the sea ice cover produced by the ocean model which contains a sea-ice model.

The procedure used to derive $\mathscr{A}$, $\mathscr{B}$ and $\mathscr{C}$ is outlined in Appendix A. 200 years daily data obtained from an ECHO-G integration are used for the derivation. Such a long integration is necessary to obtain reliable estimates of $\mathscr{A}$, $\mathscr{B}$ and $\mathscr{C}$. Since EMAD is an anomaly model, only deviations from the mean annual cycle with the period of 360 days are used. As being derived from daily data, the time step of EMAD is one day.

3 Stationary responses to different oceanic conditions

To test how EMAD reacts to different oceanic forcing, stationary responses to two idealized oceanic conditions are considered. The response patterns are given by

$$\mathbf{x} = (\mathscr{I} - \mathscr{A})^{-1} \sim \mathscr{B}\mathbf{y} \qquad (3.1)$$

where $\mathbf{y}$ represents the oceanic condition and $\mathscr{I}$ is the identity matrix. Eq.(3.1) is obtained using the stationarity condition: $\mathbf{x}_{t+1} = \mathbf{x}_t$. One can also derive the response numerically by integrating EMAD for a given constant $\mathbf{y}$. In this case, the solution will approach to Eq.(3.1) after some integration time. The response patterns discussed below are derived for a given $\mathbf{y}$ according to Eq.(3.1).

a) Stationary responses to El-Niño-related SST anomalies

The first oceanic condition considered is the first EOF of the Pacific SST in the ECHO-G integration which describes typical SST-anomalies in the tropical Pacific produced by the ECHO-G model. The maximum SST anomaly reaches 1.8° C in the eastern equatorial Pacific near 120°W.

Fig. 2a) and b) show EMAD's responses in the net heat and fresh water flux to the El-Niño SST anomalies. The heat flux anomalies are negative (upward) and characterized by two maxima located in the central and eastern tropical Pacific (near 165°W and 120°W) respectively. The structure of the heat flux anomalies in the eastern Pacific suggests that these anomalies represent upward sensible heat fluxes induced by warmer than normal SST in that region. The maximum in the central Pacific on the other hand results not only from changes in sensible heat flux, but also in short wave radiation (not shown). As indicated by Fig. 2b), EMAD produces stronger than normal precipitation in response to the SST anomalies. These precipitation anomalies lead to a reduction in the downward short wave radiation, probably via an increase in cloudiness, which contributes to the negative maxima of the net heat flux in the central Pacific.

The wind stress response pattern (not shown) reveals westerly wind stress anomalies throughout the equatorial Pacific. Large wind stress anomalies in the North Pacific are consistent with the PNA circulation pattern, which is observed to be related to the SST anomalies in the tropical Pacific.

The stationary responses are comparable with anomalies observed during an El Niño event. For instance, Fig. 2a) strongly resembles the distribution of heat flux anomalies found during the 1986-87 El Niño (SUN, 2003). Fig. 2b) is consistent with strong negative OLR values observed during 1982–83 El Niño (PHILANDER, 1990), which indicate enhanced precipitation and thus positive freshwater flux anomalies over the central tropical Pacific.

The example of EMAD's response to El Niño-related SST anomalies demonstrates that EMAD is able to produce response to SST-changes with respect to all fluxes needed by an ocean model, rather than just one particular flux. This marks one of the major differences between EMAD and the other simple models of fluxes such as Eq.(1.1) and Eq.(1.2).

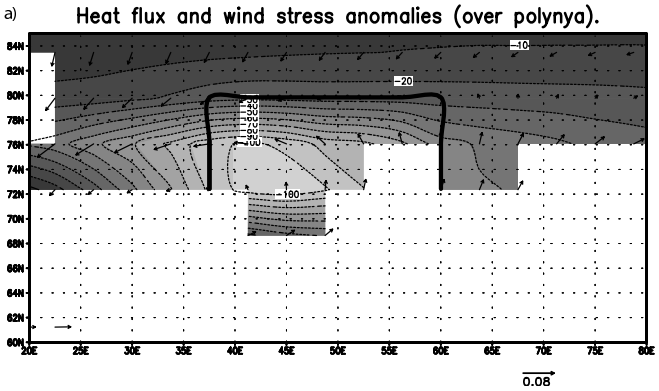

Figure 3: Stationary responses of EMAD in the region (20E-80E, 60N-84N) to a polynya in terms of the net heat flux (W/m^2) and wind stress (Pa). The polynya is marked by the box, shaded surface outside the box is ice-covered and land surface is in white.

b) Stationary responses to a polynya

The second anomalous oceanic condition is to concidered a big polynya in the Arctic. The size of the polynya is about 25° longitude by 8° latitude, indicated by the box in Fig. 3. It is placed just to the northern border that separates the domain of the water and ice modules. Within the polynya, SST is set to 0° C and the sea ice over A to zero.

EMAD responds to the polynya condition by producing anomalous upward (negative) net heat flux up to 100 W/m^2 (shading in Fig. 3). This heat source leads to an anomalous cyclonic circulation associated with anticlockwise wind stress anomalies (arrows in Fig. 3). Furthermore, it causes also stronger than normal evaporation and from that anomalous upward (negative) fresh water flux (not shown). The cyclonic anomalies and net heat loss shown in Fig. 3 are consistent with observations of BARBER et al. (2001). However, it should be noted that since weather conditions last seldom longer than a day in the polar region, Fig. 3 cannot always be directly compared with observations. For instance, the net heat flux can be downward, if the polynya is not large enough to produce sufficient clouds (BRÜMMER and Schröder, 2002).

The example of EMAD's response to the polynya condition reveals another difference between EMAD and previously used simple models. Namely EMAD generates not only fluxes over the ice-free part of the ocean, but also fluxes over regions where sea ice can be formed.

4 Second moment statistics

a) Variance distribution

Section 3 considers only the stationary responses of EMAD. It does not indicate whether or not EMAD is able to realistically represent the time-varying part of the fluxes. The latter is studied here by considering the global distribution of the total variances produced by EMAD. For this purpose, EMAD is integrated using sea surface conditions obtained from a 10-year integration with the ECHO-C coupled model. The variances calculated from such an EMAD-integration are compared with those found in the same ECHO-C integration after subtracting the mean annual cycle. It is noted that the ECHO-C model differs from the ECHO-G. The atmospheric component is the ECHAM5 model, rather than the ECHAM4 model as in ECHO-G. The oceanic component is the MPI-OM formulated on an orthogonal curvilinear 'Arakawa C'-grid which has poles over Greenland and Antarctica (MARSLAND et al. 2003). The oceanic component of the ECHO-G model on the other hand is the HOPE-G model formulated on an 'Arakawa E'-grid. The use of the ECHO-C integration provides an independent test of EMAD. Further, it is also valuable for further investigations of oceanic variations planned with the MPI-OM model coupled to EMAD.

Fig. 4 shows the variances of the zonal wind stress generated by EMAD (top panel), the ECHO-C model (middle panel) and the ECHO-G model (bottom panel). EMAD reproduces the overall distribution, characterized by large wind stress variances at the mid-latitudes in both hemispheres. Notable differences from the coupled GCM-integrations are found with respect to the maxima. The maxima in EMAD are larger than those in the two coupled GCM-integrations. This is partly due to the fact that the ECHO-G model which is used to fit the EMAD-matrices produces some what larger variances than the ECHO-C model.

However this fact alone does not completely explain the differences in maxima. There are two other possibilities which need to be considered. First, the SST data used to drive the EMAD may contain particular variations, which produce the large maximum values. To clarify this, an additional EMAD integration is carried out, in which the B-term is switched off. The variance of zonal wind stress produced by this EMAD integration is essentially identical to the top panel of Fig. 4. The result, which is consistent with the cross-correlation between SST and wind stress (see Section 4b), rules out the possible effect of SST. Secondly, the implementation of the noise-term may also alter the magnitude of the variance. Ideally, the noise should be added for each flux in $\mathbf{x}$ using all m EOFs of the residual (i.e. the part which is not described by the $\mathscr{A}$ and $\mathscr{B}$ terms, see Appendix A). In this case, one has $\mathscr{C}\mathbf{n} = \sum_{i=1}^{m} \mathbf{e}_i n_i$ with n_i being a zero-mean white noise whose variance equals the i-th eigenvalue of the covariance matrix of the residual. Since m, the number of grid points, is very large, the noise-term is implemented not using all the EOFs, but only the first 10. It can be shown that such a representation, though easier to implement, does not ensure that the noise term

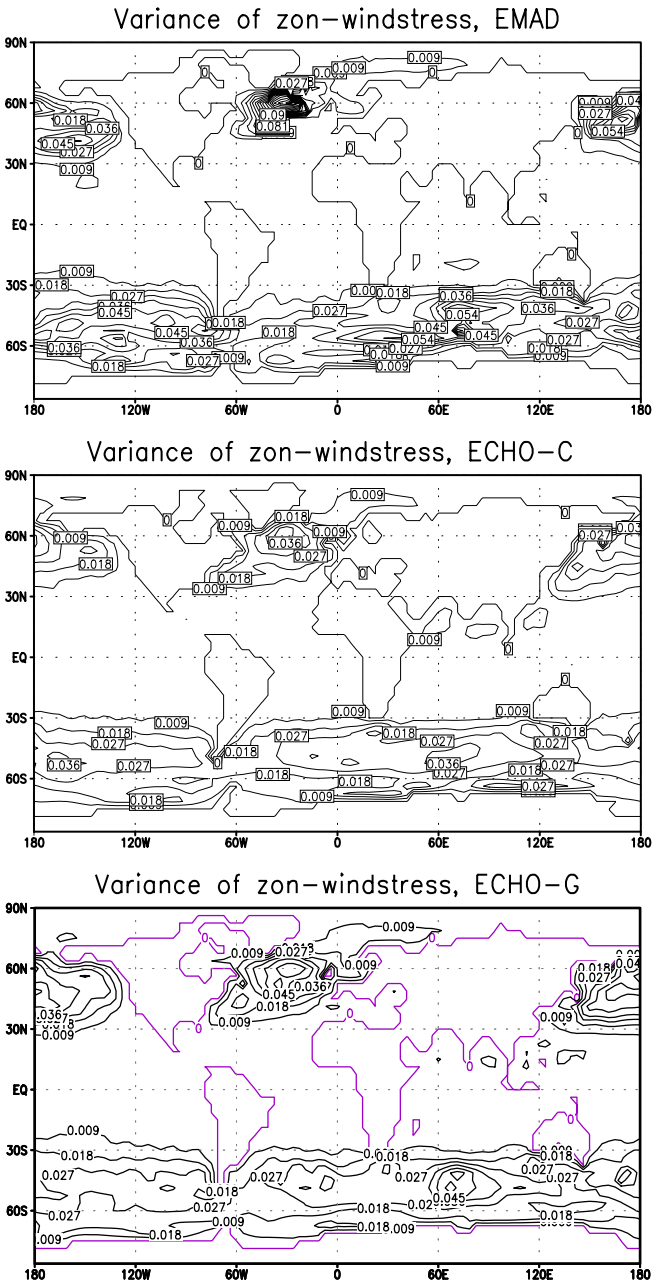

Figure 4: Variances of the zonal wind stress (Pa^2) calculated from a 10-year integration of EMAD driven by the sea surface conditions obtained from a 10-year ECHO-C integration (top), the same 10-year integration with the ECHO-C model (middle) and a 10-year integration with the ECHO-G model (bottom).

has exactly the same covariance matrix as the residual. The difference concerning the maximum values could be produced by such a noise implementation.

For the heat flux, the variance is found to be larger in the EMAD run than in the ECHO-C run over most of the Southern Oceans, but vice versa in the western North Pacific and western North Atlantic (not shown). The shape of cross-correlation function between SST and heat flux (see Section 4b) underlines the importance of the term $\mathscr{B}$, that describes the response of heat flux to SST, for the generation of the heat flux. This suggests that relative to the ECHO-C heat flux, the EMAD heat flux responds stronger to SST anomalies in the North Atlantic and in the North Pacific, but less strong in the Southern Oceans. Due to the dominant role of SST, the error induced by the noise implementation is less severe for heat flux than for wind stress.

Overall, despite of the detailed differences, the general structures of the variances obtained from the EMAD-run are comparable to those obtained from the ECHO-C run.

b) Cross-correlation functions between SST and fluxes

In the EMAD run driven by the sea surface conditions from ECHO-C, the SST anomalies are allowed to affect the fluxes, but the fluxes are unable to change the SST. To further check the interactions between the fluxes and the sea surface conditions, EMAD is coupled to the HOPE-G O-GCM via OASIS (VALCKE et al., 2000) and cross-correlations between SST and fluxes are calculated from the EMAD/HOPE-G integration and compared with those obtained from a 50-year piece of the ECHO-G integration, that was not used to derived the EMAD. The EMAD/HOPE-G model is integrated for 10 years. In the new phase of the project, EMAD will be coupled to the MPI-OM model with the curvilinear coordinate. This however requires an extra interpretation between the T30 grid on which EMAD is built and the curvilinear grid of the MPI-OM. Once this is complete, longer integrations will be carried out with the EMAD/MPI-OM model.

Fig. 5 shows the cross correlation functions between SST and heat flux (top panel) and SST and zonal wind stress (bottom panel) at three extratropical grid points in the ECHO-G run (left) and at the same grid points in the EMAD/HOPE-G run (right).

The anti-symmetric shape of the cross-correlations between SST and the heat flux is characteristic over most part of the model ocean. It suggests that the heat flux acts to generate SST anomalies and these anomalies, once being generated, are damped by the heat flux. This type of interaction which cannot be described by restoring condition as given in Eq.(1.1) is reproduced by the EMAD.

In the extratropical region, the interaction between SST and the zonal wind stress is characterized by the vanishing correlation between SST and wind stress when SST leads. This suggests that the feedbacks of SST anomalies to the wind stress are negligible. This type of interaction which cannot be described by Eq.(1.2) is reproduced by the EMAD.

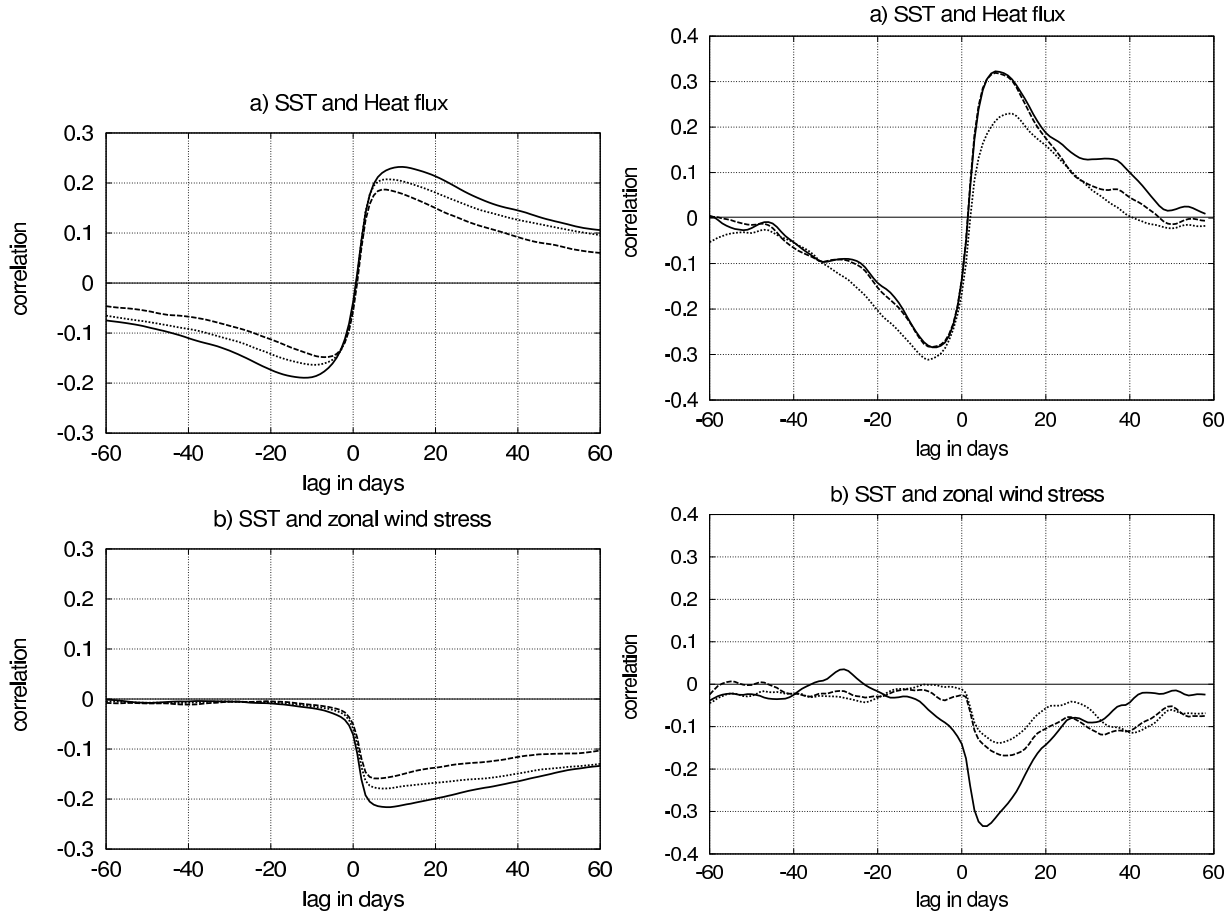

Figure 5: Cross-correlation functions between SST and the net heat flux (top) and between SST and zonal wind stress (bottom) at three grid points which are in North Atlantic, North Pacific and South Pacific respectively. The correlation functions are derived from a 10-year EMAD/HOPE-G integration (right) and a 50-year ECHO-G integration (left).

5 Concluding remarks

This paper introduces an empirical model which optimally represents the time-varying part of the fluxes at the sea surface. The model is based on the general structure given in Eq.(2.1), that allows different types of air-sea interactions, depending on the relative dominance of the model parameters. The parameters are fitted to a long integration with the coupled ECHO-G model which parameterize the fluxes in a realistic (rather than ad hoc) manner. The such derived model reacts to different sea surface conditions, produces variance distributions comparable to those obtained from a coupled AO-GCM, and reproduce characteristic air-sea interactions as suggested by the cross-correlation functions. The proposed empirical model can be updated, when long and complete observational records or integrations with improved coupled AO-GCM are available.

The present model differs from the previous simple models in various respects. It deals with all fluxes required to drive an OGCM, rather than concentrating on one flux as in Eq.(1.1) and Eq.(1.2). Furthermore, different from the previous simple models which leave the sea ice problem out, the present model operates in regions where sea ice can be formed and produces fluxes required to update the formation and melting of sea ice. Finally, the present model allows different types of interactions to occur for different fluxes and in different geographical regions. It can be used in place of an AGCM to drive an O-GCM. Last but not least, the analyses which lead the formulation of EMAD provide a quantitative description of air-sea interaction processes produced by the coupled AO-GCM.

In the next phase of the "Sonderforschungsbereich", the here developed EMAD model will be used to study the oceanic variations. This can be done by performing integrations with MPI-OM coupled to different versions of EMAD, e.g. one with all three terms in Eq.(2.1) and one with only the $\mathscr{A}$- and $\mathscr{C}$-term. The differences in oceanic variations identified in the two integrations can be used to assess the question of whether the oceanic variations are coupled modes which involve active air-sea interactions or damped ocean modes which are generated stochastically without oceanic feedbacks.

Acknowledgements

This work is supported by the Deutsche Forschungsgemeinschaft in the Sonderforschungsbereich 512, "Tiefdruckgebiete und Klimasystem des Nordatlantiks".

6 Appendix A: Derivation of matrices $\mathscr{A}$, $\mathscr{B}$ and $\mathscr{C}$

The matrices $\mathscr{A}$ and $\mathscr{B}$ are derived in the EOF-space. For this purpose, each flux in $\mathbf{x}$ and each sea surface variable in $\mathbf{y}$ are projected into their corresponding EOF-space. $\mathbf{p}_{x,t}$ and $\mathbf{p}_{y,t}$ compose the principle components of all fluxes contained in $\mathbf{x}$ and all sea surface variables contained in $\mathbf{y}$ at t. The one-time-step prediction by EMAD in the EOF-space reads

$$\hat{\mathbf{p}}_{x,t+1} = \mathscr{A}\mathbf{p}_{x,t} + \mathscr{B}\mathbf{p}_{y,t}.$$

where $\hat{\mathbf{p}}$ indicates the principle components predicted by the EMAD. The matrices $\mathscr{A}$ and $\mathscr{B}$ are obtained by minimizing the mean squared differences between the principle components predicted by the deterministic part of the EMAD, $\hat{\mathbf{p}}_{x,t}$, and the true principle components (as obtained from an integration with a coupled AO-GCM), $\mathbf{p}_{x,t}$,

$$< (\mathbf{p}_{x,t} - \hat{\mathbf{p}}_{x,t})^2 >= min.$$

As the solution of the minimization, one obtains

$$\mathscr{A} = (\Sigma_1{}^T - \mathscr{C}_1{}^T\Pi^{-1}\mathscr{C}_0)(\Sigma_0{}^T - \mathscr{C}_0{}^T\Pi^{-1}\mathscr{C}_0)^{-1},$$

$$\mathscr{B} = (\mathscr{C}_1{}^T - \mathscr{A}\mathscr{C}_0{}^T)\Pi^{-1}$$

where ^{T} denotes transpose and $^{-1}$ denotes inverse. Σ_1 is the lag-1 covariance matrix, Σ_0 the lag-0 covariance matrix of $\mathbf{p}_x$. Π is the lag-0 covariance matrix of $\mathbf{p}_y$. As PCs are used for the minimization, Σ_0 and Π are diagnonal. $\mathscr{C}_0$ denotes the lag-0 cross-covariance matrix of $\mathbf{p}_x$ and $\mathbf{p}_y$, $\mathscr{C}_1$ the cross-covariance matrix at lag one.

Given $\mathscr{A}$ and $\mathscr{B}$, $\mathscr{A}\mathbf{p}_{x,t} + \mathscr{B}\mathbf{p}_{y,t}$ can be transformed into the grid point space for each t. Denote the resulting time series for a flux by $\hat{\mathbf{x}}_t$. The residual of this flux which is not described by the deterministic part of the EMAD is

$$\mathbf{x}_t - \hat{\mathbf{x}}_t = \zeta_t.$$

The matrix $\mathscr{C}$ is determined such that $\mathscr{C}\mathbf{n}$ with $\mathbf{n} = (n_1, \cdots, n_m)^{-1}$ being a zero-mean multivariate white noise describes the covariances of the residual time series ζ_t.

This is the case, when

$$\mathscr{C} = (\mathbf{e}_1, \mathbf{e}_2, ...\mathbf{e}_m),$$

where $\mathbf{e}_i$ with $i = 1, \cdots, m$ are EOF's of ζ_t, and the variance of the i-th component of $\mathbf{n}$ equals the eigenvalue λ_i that corresponds to eigenvector $\mathbf{e}_i$. In this case, the covariance matrix of $\mathscr{C}\mathbf{n}$ equals the covariance matrix of ζ.

References

BARBER, D.G., J.M. HANESIAK, W. CHAN, J. PIWOWAR, 2001: Sea-Ice and Meteorological Conditions in Northern Baffin Bay and the NOW polynya between 1979 and 1996. – Atmosphere-Ocean **39**, 343–359.

BRÜMMER, B., D. SCHRÖDER, 2002: Temporal and spatial variability of surface fluxes over the ice edge zone in the northern Baltic Sea. – J. Geophy. Res. **107**, 101029.

FRANKIGNOUL, C., 1985: Sea surface temperature anomalies, planetary waves, and air-sea feedbacks in the middle latitudes. – Rev. Geophy. **23**, 357–390.

FRANKIGNOUL, C., A. CZAJA, B. L'HEVEDER, 1998: Air-sea feedback in the North Atlantic and surface boundary conditions for ocean models. – J. Climate **11**, 2310–2324.

LATIF, M., A. VILLWOCK, 1990: Interannual variability as simulated in coupled ocean-atmosphere models. – J. Mar. Systems **1**, 51–60.

LEGUTKE, S., R. VOSS, 1999: The Hamburg atmosphere-ocean coupled circulation model ECHO-G. – DKRZ-Report **18**, Hamburg, Germany.

MARSLAND, S.J., J. HAAK, J.H. JUNGCLAUS, M. LATIF, F. ROESKE, 2003: The Max-Planck-Institut global ocean/sea ice model with orthogonal curvilinear coordinates. – Ocean Modelling **5**, 91–127.

PHILANDER, S. G., 1990: El Niño, La Niña, and Southern Oscillation. – Academic Press, San Diago, California. 293 pp.

RAIBLE, C., U. LUKSCH, K. FRAEDRICH, R. VOSS, 2001: North Atlantic decadal regimes in a coupled GCM simulation. – Climate Dyn. **18**, 321–330.

SUN, DE-ZHENG, 2003: A possible effect of an increase in the warm pool SST on the magnitude of El Niño warming. – J. Climate **16**, 185–205.

VALCKE, S., L. TERRAY, A. PIACENTINI, 2000: Oasis 2.4, Ocean Atmosphere Sea Ice Soil: User's guide. – CERFACS Technical Report TR/CMGC/03/69, CERFACS, Toulouse, France.

VON STORCH, J.-S., 2000: Signatures of air-sea interactions in a coupled atmosphere-ocean GCM. – J. Climate **13**, 3361–3379.